A Broadband Low-RCS Circularly Polarized Meta-Antenna

Hongkun Zhou, Yuchao Wang, Chengguo Liu* and Cheng Zhang*

Hubei Engineering Research Center of RF-Microwave Technology and Application, School of Science, Wuhan University of Technology, Wuhan, China

A low-profile circularly polarized (CP) meta-antenna with a broadband low-RCS feature is proposed in this article. Our design is the combination of a CP antenna with a chessboard polarization conversion metasurface (CPCM) for balancing the radiation property and stealth feature. To relieve the adverse effect of the CPCM on the entire radiation performance, several redundant meta-atoms with the opposite phase state were removed to enhance the realized gain within the operation bandwidth (8.0–9.0 GHz). The proposed meta-antenna showed excellent radiation performance: −10 dB impedance relative bandwidth was 26.48% (6.78–8.85 GHz), and 3-dB axial ratio relative bandwidth was 22.03% (7.27–9.07 GHz). In addition, RCS reduction over 5 dB was achieved *via* our design from 8.5 to 21.5 GHz (86.67%) with the help of the deliberately designed CPCM. The final measured results demonstrate great consistency with the simulated ones.

Keywords: low profile, circularly polarized, broadband, radar cross-section reduction, meta-antenna

INTRODUCTION

In recent years, antennas with a wideband low radar cross section (RCS) have drawn significant attention in the low-observable needed platforms, such as military aircraft and missiles. Traditional strategies to reduce the RCS of the antennas are shape design or adding absorbers such as metamaterial absorbers [1, 2], frequency-selective surfaces/absorbers (FSS/FSA) [3–5], and electromagnetic bandgap structures [6] onto the antennas. Through these methods, the backward RCS can be confined to certain extent, while the radiation performances, including the working bandwidth and realized gain, are difficult to be maintained. For instance, in Ref. [5], an FSA was adopted in a 4 × 4-array antenna to restrain the normal reflection from the whole structure by an average of 11 dB (from 4.41 to 5.43 GHz) by absorbing the incident electromagnetic waves. But the antenna could only work at the same bandwidth. To further improve the stealth performance, a low-RCS Fabry–Perot (FP) antenna was proposed in Ref. [7], in which a partially reflecting surface was utilized to achieve low RCS (over 4 dB from 6 to 14 GHz). However, the operation bandwidth of the antenna further shrunk. From the previous discussions, it is easy to find that obtaining a good radiation feature and broadband stealth performance at the same time is challenging.

Nowadays, the prompt development of metasurfaces [8–10] provides an alternative and potential strategy to address the aforementioned problem. Compared to the traditional methods, the polarization conversion metasurface (PCM) has been widely used to design low-RCS devices [11, 12], of which through optimizing the polarization conversion (PC) bandwidth and the polarization conversion ratio of the corresponding meta-atoms, the operation bandwidth for RCS reduction can be flexibly controlled as desired. Therefore, several attempts have been taken to design a low-RCS meta-antenna while not affecting its radiation performance. In Ref. [11], a chessboard polarization conversion metasurface (CPCM) was used in a slot array antenna, and its RCS reduction over 5 dB was achieved from 6 to 18 GHz. In the meantime, a dumbbell CPCM

FIGURE 1 | (A) Top view and side view of a typical unit cell. (B) The reflection phase of the unit cell and its mirror. (C) Co- and cross-polarized reflection coefficients and PCR of the proposed meta-atom.
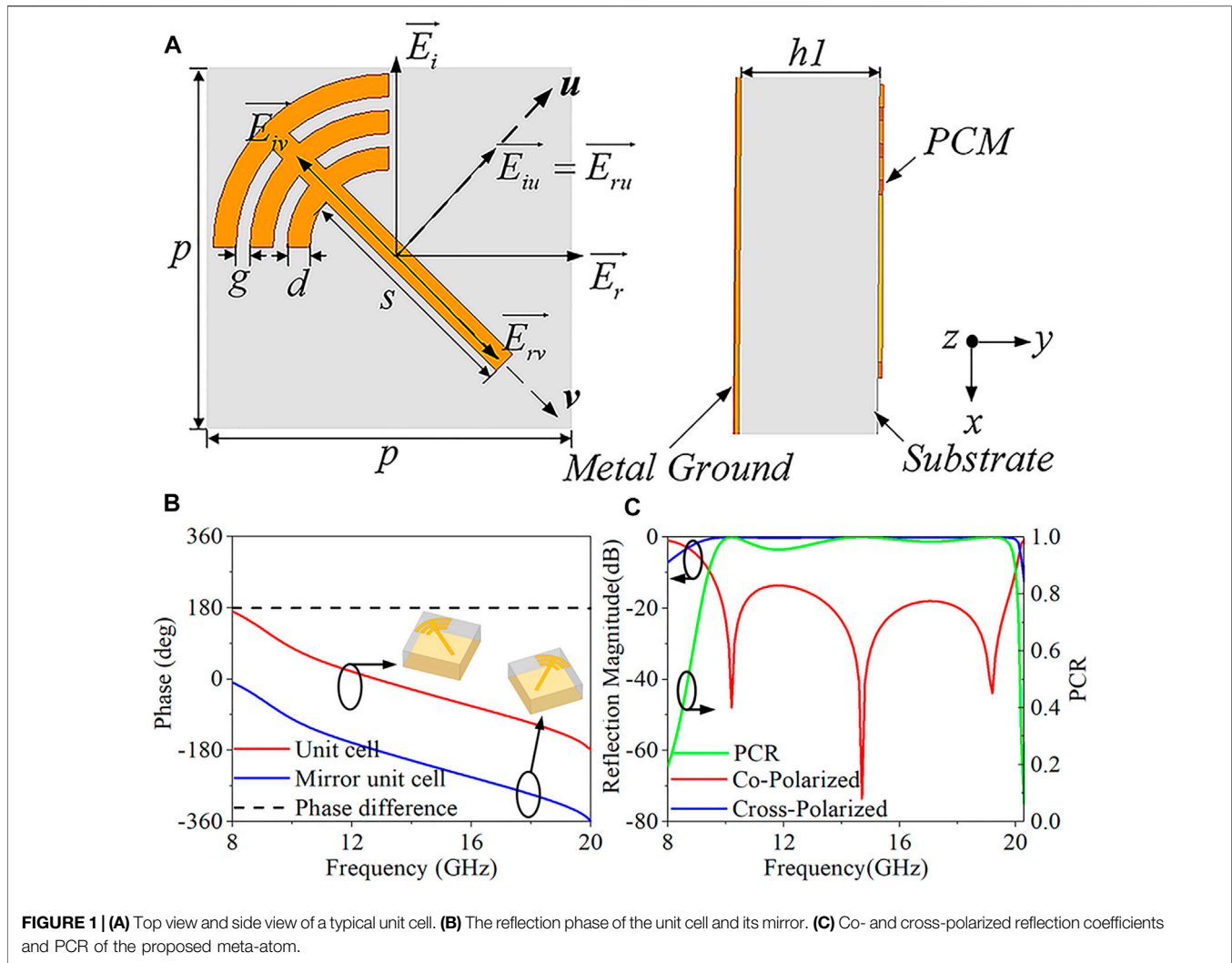
applied to an FP antenna was proposed in Ref. [12], which achieved an RCS reduction bandwidth of 8–26 GHz and an antenna operating bandwidth of 8.41–12.11 GHz. In addition, most of the reported low-RCS antennas just can interact with the linearly polarized waves [12, 13], but only a few circularly polarized (CP) antennas have been investigated. More attention should be paid to low-RCS CP antennas due to their widespread applications such as radar, communication, and sensor systems. Several attempts have been made to solve this problem. For example, in Ref. [14], a gain of 3.5 dB and impedance bandwidth of 500 MHz were achieved *via* placing a CPCM onto a patch antenna; however, the RCS reduction bandwidth only covered a frequency range of 9–13 GHz. In Ref. [15], RCS reduction over 6 dB was achieved at 4.95–15.73 GHz as the CP patch antenna was loaded with a CPCM, but the reflection coefficient increased from −30 dB to −20 dB compared to the reference antenna without a CPCM. Hence, there is still a need for a plentiful effort to be made for developing a CP antenna with a good stealth feature and excellent radiation performance.

In this article, a low-profile CP circular patch meta-antenna is proposed. With the help of the elaborately designed CPCM, our design can achieve good RCS reduction performance within an ultra-wideband frequency range. CP performance of the proposed meta-antenna was achieved by a feed network consisting of a Wilkinson power divider and a 90° broadband phase shifter. Meanwhile, slots were cut in the patch to increase the axial bandwidth. It is worthy to note that the radiation performance of the antenna was still maintained even after loading the CPCM.

DESIGN AND ANALYSIS OF THE CPCM

The schematic diagram of the proposed meta-atom is illustrated in **Figure 1A**. The unit cell comprises a top metallic pattern and a bottom metallic ground plane with a dielectric substrate between them. The top layer is the PC structure that consists of a quarter of three adjacent rings and a rectangular strip. The dielectric layer adopts an F4B substrate (a relative dielectric constant of 2.2) with
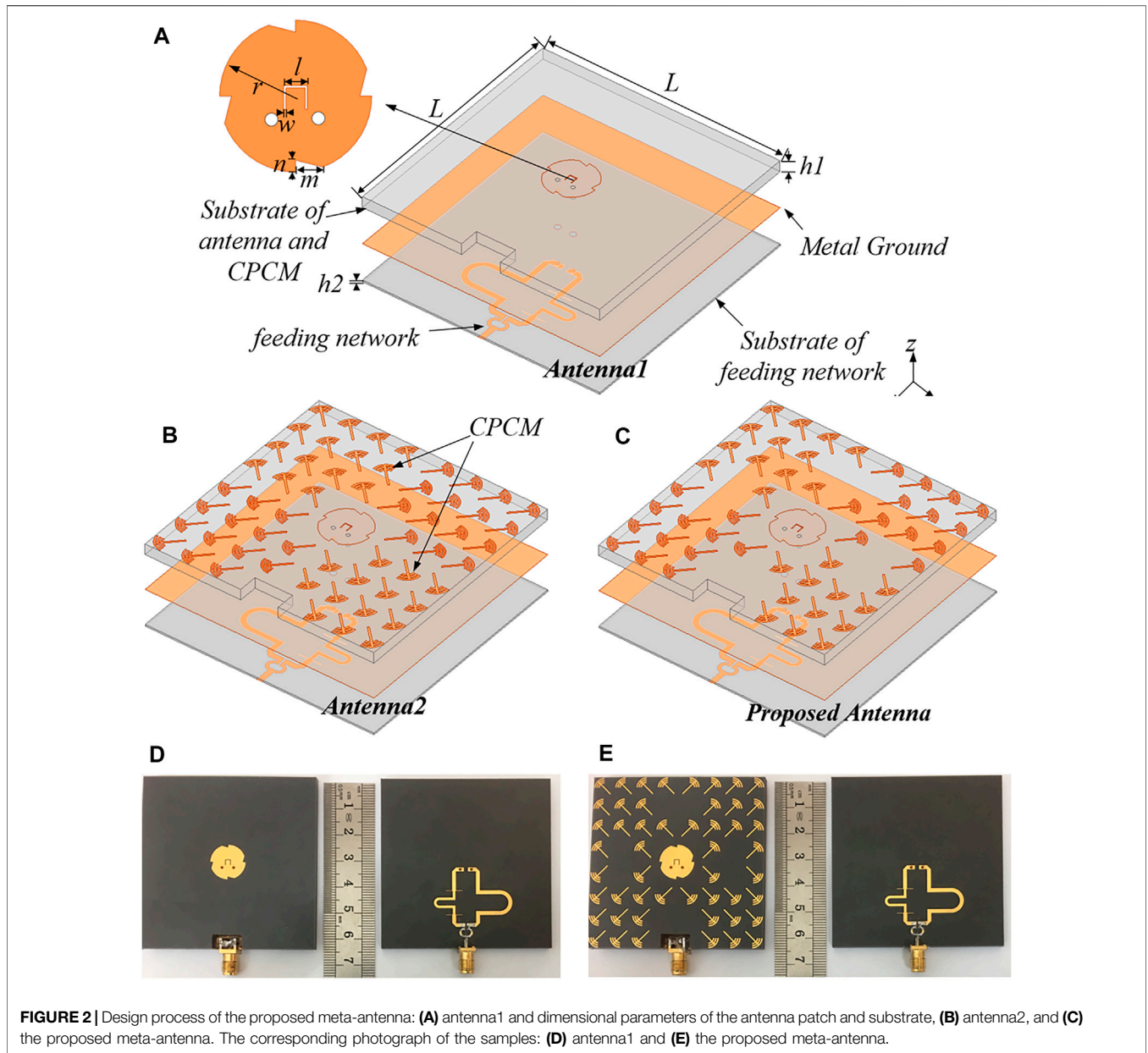
FIGURE 2 | Design process of the proposed meta-antenna: **(A)** antenna1 and dimensional parameters of the antenna patch and substrate, **(B)** antenna2, and **(C)** the proposed meta-antenna. The corresponding photograph of the samples: **(D)** antenna1 and **(E)** the proposed meta-antenna.

a thickness of 3 mm. The typical geometrical parameters of the unit cell are as follows: $s = 8.5$ mm, $d = 0.3$ mm, $p = 8$ mm, and $g = 0.2$ mm. Electromagnetic simulation software HFSS was used to calculate the performance of the unit cell by using Mater/Slaver boundary conditions.

In **Figure 1A**, to investigate the PC response of the proposed unit cell, the electric field $\vec{E}_i$ of the x-polarized incident wave was decomposed into two components $\vec{E}_{iu}$ and $\vec{E}_{iv}$. When the electric fields were along the u- and v-axis (135° and 225° from x-axis), the magnitudes of the two reflected fields $\vec{E}_{ru}$ and $\vec{E}_{rv}$ were almost the same. Therefore, the total reflected electric field $\vec{E}_r$ is vertical to the x-axis with the same magnitude as $\vec{E}_i$. For the chessboard arrangement, the mirror unit cell also has a reflected electric field of the same magnitude, and the

reflection phase difference between the unit cell and its mirror was nearly 180°, as shown in **Figure 1B**. Under the illumination of electromagnetic waves, the scattering pattern of the CPCM can be determined by the superposition of far fields from the unit cells by using the following formula [16, 17]:

$$f(\theta,\varphi) = f_e(\theta,\varphi)\sum_{m=1}^{M}\sum_{n=1}^{N}\exp\left\{-i\left\{\varphi(m,n)+k_0 p\sin\theta\right.\right.$$
$$\left.\left.\left[(m-1/2)\cos\varphi+(n-1/2)\sin\varphi\right]\right\}\right\}, \quad (1)$$

where m and n are the row and column numbers in the CPCM, respectively. p is the element periodicity. θ, φ, and k_0 are the
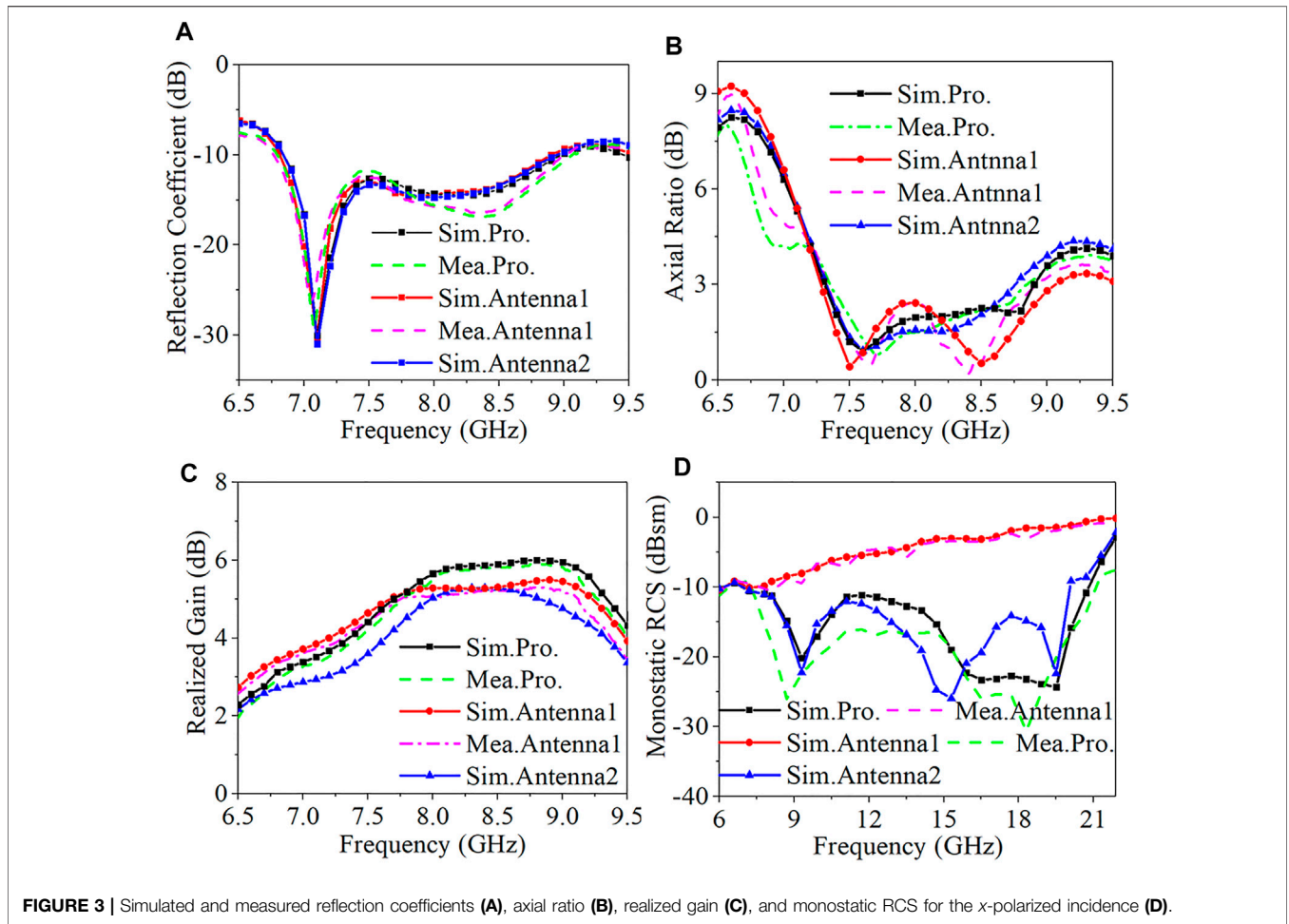
FIGURE 3 | Simulated and measured reflection coefficients **(A)**, axial ratio **(B)**, realized gain **(C)**, and monostatic RCS for the *x*-polarized incidence **(D)**.

elevation angle, azimuth angle, and wavenumber of the free space, respectively. $\varphi(m, n)$ is the reflection phase of the lattice (m, n), and $f_e(\theta, \varphi)$ is the pattern function of a single unit. Indeed, the scattering beam can be adjusted by inverting the unit cell phase by iterating a fast Fourier transform. Therefore, phase cancellation of the reflected electric field and reduction of RCS can be achieved by the CPCM.

Co-polarized and cross-polarized reflection coefficients with *x*-polarized incident waves are illustrated in **Figure 1C**. It can be seen that the operating band (where the co-polarization reflection coefficient is less than –10 dB) of the meta-atom is from 9.46 to 20.01 GHz. The polarization conversion ratio (PCR) is used to describe electromagnetic polarization rotation and is defined as the ability to convert *x*- or *y*-polarized waves into cross-polarized waves that can be expressed as

$$PCR = |R_{cross}|^2 / (|R_{cross}|^2 + |R_{co}|^2), \qquad (2)$$

where R_{co} and R_{cross} represent the reflection coefficient of co- and cross-polarization, respectively. The operating band was from 9.46 to 20.01 GHz as the value of the PCR was greater than 90%, which illustrates that more than 90% of the linearly polarized incident power can be converted into cross-polarized power.

META-ANTENNA DESIGN

Figure 2 shows the geometry and design process of the CP patch meta-antenna. The entire size of the meta-antenna is 64 mm × 64 mm × 3.5 mm. As depicted in **Figure 2A**, the antenna is designed with double dielectric plates (F4B). The antenna is composed of a patch, ground, and the feeding network. The top patch and the bottom feeding network are connected *via* two holes. Below the metal ground, the feeding network consisting of a Wilkinson power divider and a 90° broadband phase shifter was mounted on the bottom substrate with a thickness of h_1. The Wilkinson power divider can achieve equal power division and impedance by transforming between input and output ports. After the original input signal splits into two ways, they pass through the two paths of the 90° phase shifter to obtain a stable phase shifting. In this design, a pair of 8/λ open and short lines was deployed to smooth the phase variation, where λ is the wavelength of the center frequency (8 GHz) on the substrate. All ports of the divider were matched to 50 Ω. The isolation between the two outputs was determined by a 100-Ω chip resister. Therefore, the CP radiation was achieved by generating two output signals with equal amplitude and 90°

FIGURE 4 | Phase distribution of antenna2 at 7.5 GHz **(A)** and 8 GHz **(B)**. Surface current vector distribution of the proposed meta-antenna in the radiation case at 8 GHz: **(C)** phase = 0° and **(D)** phase = 90°.
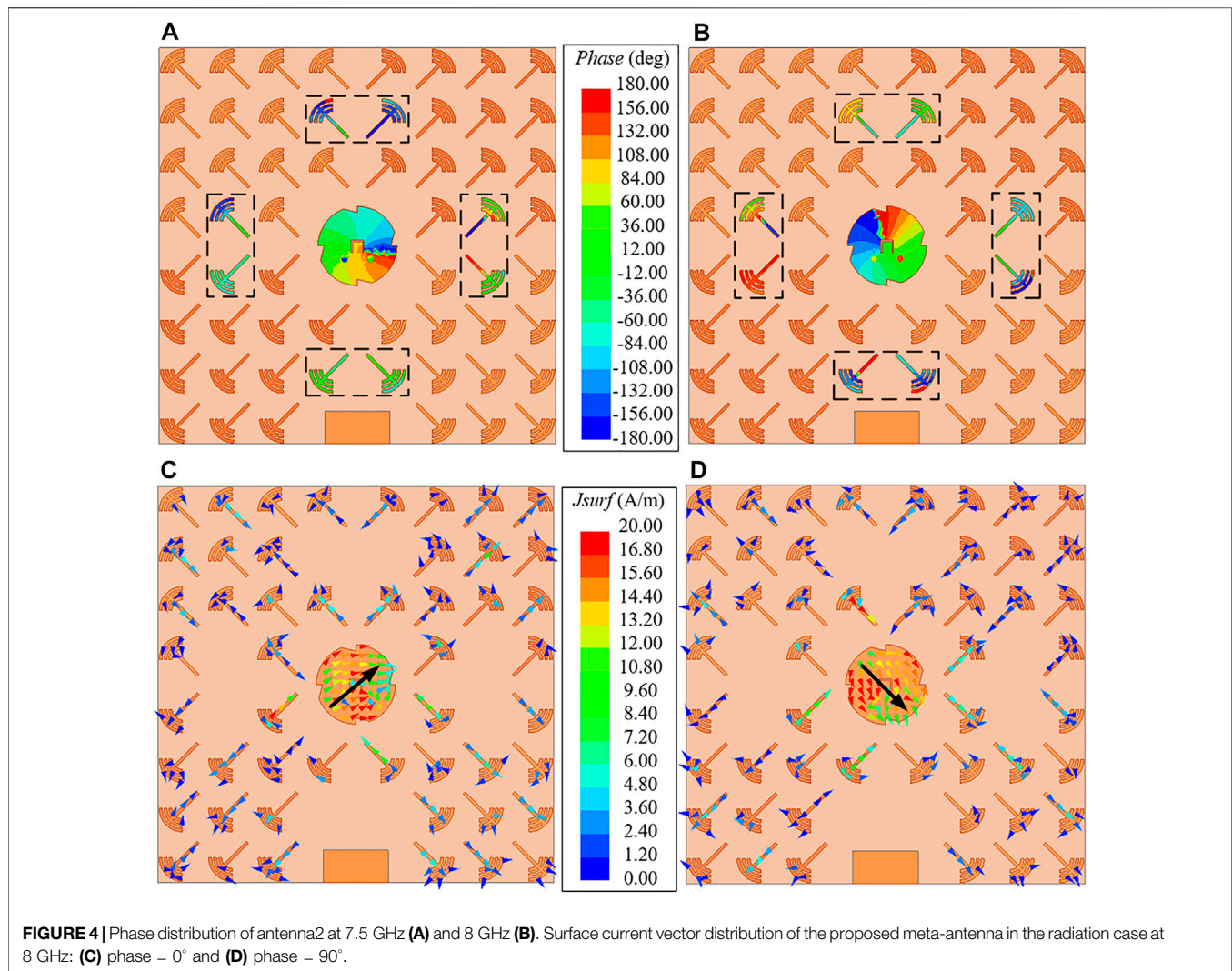
phase difference of the feeding network. In addition, a U-shaped slot and four triangular slots were cut on the circular patch. The function of the U-slot is to introduce a capacitance that can suppress the inductance induced *via* the holes and to enhance the impedance and axial-ratio bandwidths. Four triangular slots were embedded to further reduce the size of the antenna. The CP slotted patch antenna was simulated by the electromagnetic simulation software HFSS and measured in the microwave anechoic chamber. The dimensional parameters of the antenna patch and the substrate are as follows: $L = 64$ mm, $r = 6.8$ mm, $l = 2$ mm, $w = 0.2$ mm, $m = 4$ mm, $n = 1$ mm, $h_1 = 3$ mm, and $h_2 = 0.5$ mm.

The design process of the low-RCS meta-antenna is shown in **Figures 2A–C**. First, a CP slotted patch antenna was designed as the basic model shown in **Figure 2A**. The PC meta-atoms and their mirrors were arranged around the original antenna in a chessboard pattern to reduce the RCS of the whole structure, as shown in **Figure 2B**. In order to improve the radiation performance, some unit cells on the aperture were removed to relieve the coupling between the

CPCM and the patch (**Figure 2C**). To demonstrate the performance of the proposed meta-antenna, the simulated and measured results were compared with those of the reference antenna without the CPCM. The antenna1 and the proposed meta-antenna were fabricated as shown in **Figure 2** and **Figure 2E**, respectively. It should be emphasized that considering the good contact between the SMA connector and the metal ground, a 10 mm × 5 mm × 3 mm slot was cut at the edge of the substrate with a thickness of h_2, which had a little effect on the radiation performance.

The simulated and measured reflection coefficients and axial ratios of antennas are shown in **Figures 3A,B**. The relative operation bandwidth of proposed meta-antenna and antenna1 were 26.48% (6.78–8.85 GHz) and 27.05% (6.84–8.98 GHz), respectively. The 3-dB axial ratio bandwidth of our design and antenna1 were 22.03% (7.27–9.07 GHz) and 19.39% (7.31–8.88 GHz). The realized gain is shown in **Figure 3C**, and the peak realized gain was 6.01 dB at 8.8 GHz. Furthermore, at 8.0–9.0 GHz, the realized gain of the proposed antenna increased by 1dB compared with that of the

FIGURE 5 | Simulated and measured 2D radiation patterns of the proposed meta-antenna at 8 GHz (**(A)** for *xoz*-plane; **(C)** for *yoz*-plane) and antenna1 (**(B)** for *xoz*-plane; **(D)** for *yoz*-plane).
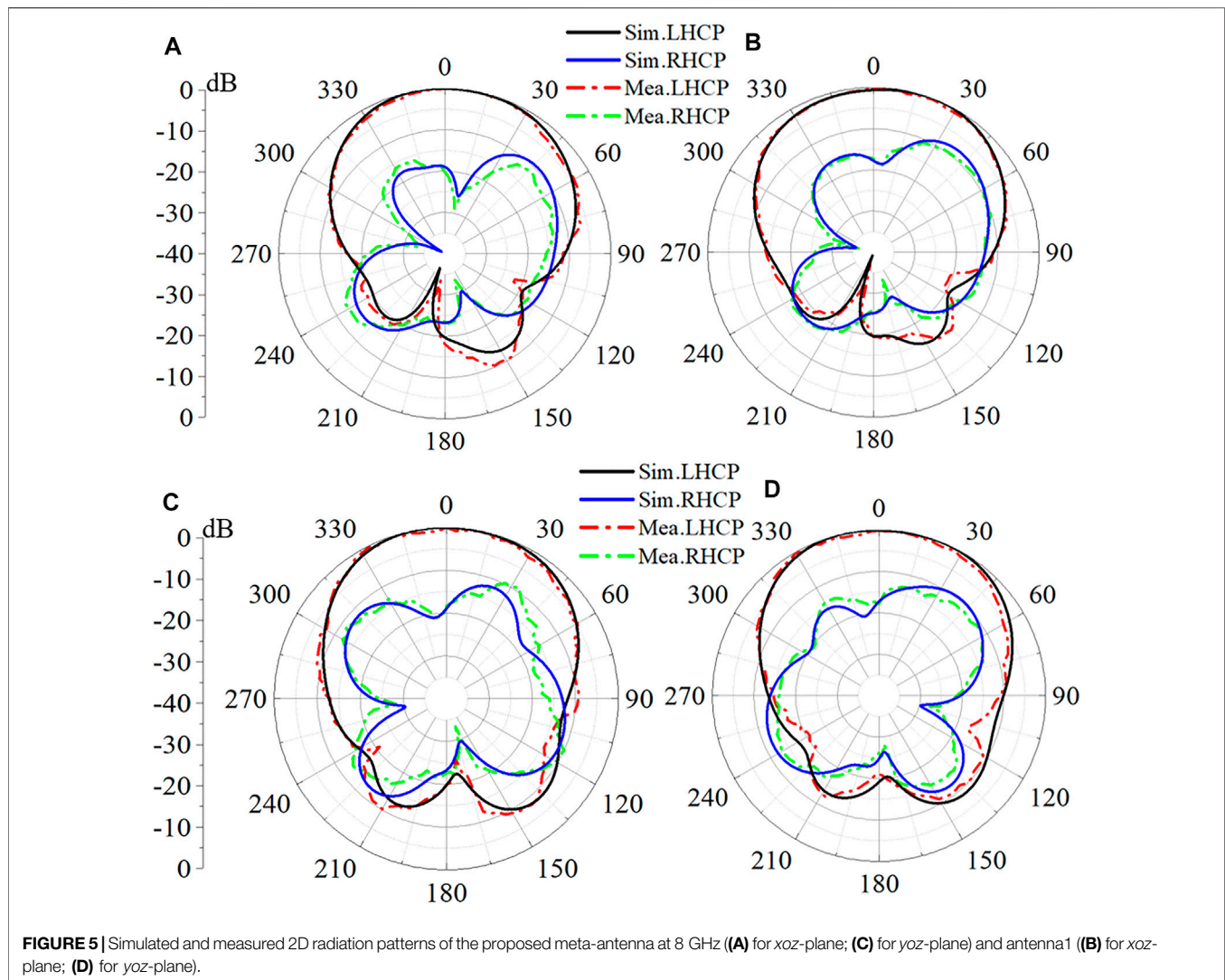
antenna1. The simulated and measured monostatic RCS are shown in **Figure 3D**. Compared with the reference antenna1, the proposed meta-antenna can achieve RCS reduction over 5 dB ranging from 8.5 to 21.5 GHz, which covers the working bandwidth of the proposed antenna. The peak RCS reduction at 19.4 GHz was 34.3 dB.

Referring to the results of antenna2 in **Figures 3A–D**, it is shown that placing a complete CPCM around an antenna has little influence on the return loss and axial ratio, but the gain of the antenna decreases by 1 dB at 7–7.75 GHz and 8.85–9.15 GHz without a CPCM because an inverting electric field is excited by several meta-atoms. The phase distribution of antenna2 at 7.5 and 8 GHz is shown in **Figure 4A** and **Figure 4B**, respectively. Therefore, to improve the realized gain of the meta-antenna, eight unit cells that are located at 0.5λ away from the center of our design have been removed since they are oppositely phased with the surrounding counterparts. In addition, compared with antenna2, the RCS of the proposed meta-antenna has improved by about 4.1 dB on an average from 11.1 to 15.8 GHz by following the aforementioned procedure. In the

meantime, the current distribution of antenna1 and the proposed meta-antenna at 8.0 GHz is shown in **Figure 4C** and **Figure 4D**, respectively. The proposed meta-atoms act as parasitical radiators due to the coupling between the patch and CPCM in the radiation case. Two orthogonal modes with 90° phase difference were excited to obtain left-hand circularly polarized (LHCP) radiation. Hence, the improvement of the radiation aperture, namely, redistributing the meta-atoms, proves to be a vital function for the gain enhancement.

The LHCP and right-hand circularly polarized (RHCP) radiation patterns of the proposed meta-antenna and the reference antenna at 8 GHz are shown in **Figure 5**. It can be seen that the main polarization is LHCP, which is consistent with the current vector distribution in **Figure 4**. The measured cross-polarization levels in both *xoz*-plane and *yoz*-plane were about 20 dB lower than co-polarizations. Moreover, the front-to-back ratios remained better than 20 dB at 8 GHz.

In comparison, the performance of the proposed meta-antenna approached that of the antenna1, and the measured

data are in good agreement with the simulation results. Some little differences are mainly due to the following reasons: I) machining and fabrication errors, II) interference of measurement environment and instrument settings, and III) the SMA and cable loss. In summary, the comparison of the above results shows that the CPCM causes little degradation in antenna radiation performance.

CONCLUSION

A CP slotted patch meta-antenna is presented in this article for reducing the backward RCS with the help of the predesigned CPCM. The measured results show that the proposed meta-antenna has an operating bandwidth of 6.79–9.06 GHz and 3-dB axial ratio bandwidth of 7.35–8.85 GHz, and the measured RCS reduction of more than 9 dB was achieved from 8.3 to 21.1 GHz without disturbing the radiation performance. Our design reached a good balance between the radiation feature and broadband stealth performance, and shows great prospects in practical applications.

REFERENCES

1. Liu T, Cao X, Gao J, Zheng Q, Li W, Yang H. RCS Reduction of Waveguide Slot Antenna with Metamaterial Absorber. *IEEE Trans Antennas Propagat* (2013) 61(3):1479–84. doi:10.1109/TAP.2012.2231922

2. Liu Y, Zhao X. Perfect Absorber Metamaterial for Designing Low-RCS Patch Antenna. *Antennas Wirel Propag Lett* (2014) 13:1473–6. doi:10.1109/LAWP.2014.2341299

3. Wang W-T, Gong S-X, Wang X, Yuan H-W, Ling J, Wan T-T. RCS Reduction of Array Antenna by Using Bandstop FSS Reflector. *J Electromagn Waves Appl* (2009) 23(11):1505–14. doi:10.1163/156939309789476473

4. Genovesi S, Costa F, Monorchio A. Low-Profile Array with Reduced Radar Cross Section by Using Hybrid Frequency Selective Surfaces. *IEEE Trans Antennas Propagat* (2012) 60(5):2327–35. doi:10.1109/TAP.2012.2189701

5. Han Y, Zhu L, Bo Y, Che W, Li B. Novel Low-RCS Circularly Polarized Antenna Arrays via Frequency-Selective Absorber. *IEEE Trans Antennas Propagat* (2020) 68(1):287–96. doi:10.1109/TAP.2019.2939845

6. You-Quan Li Y, Hui Zhang H, Yun-Qi Fu Y, Nai-Chang Yuan N. RCS Reduction of Ridged Waveguide Slot Antenna Array Using EBG Radar Absorbing Material. *Antennas Wirel Propag Lett* (2008) 7:473–6. doi:10.1109/LAWP.2008.2001548

7. Pan W, Huang C, Chen P, Ma X, Hu C, Luo X. A Low-RCS and High-Gain Partially Reflecting Surface Antenna. *IEEE Trans Antennas Propagat* (2014) 62(2):945–9. doi:10.1109/TAP.2013.2291008

8. Zhang C, Long C, Yin S, Song RG, Zhang BH, Zhang JW, et al. Graphene-Based Anisotropic Polarization Meta-Filter. *Mater Des* (2021) 206:109768. doi:10.1016/j.matdes.2021.109768

9. Zhang C, Yin S, Long C, Dong BW, He D, Cheng Q. Hybrid Metamaterial Absorber for Ultra-low and Dual-Broadband Absorption. *Opt Express* (2021) 29(9):14078–86. doi:10.1364/OE.423245

10. Zhang C, Cheng Q, Yang J, Zhao J, Cui TJ. Broadband Metamaterial for Optical Transparency and Microwave Absorption. *Appl Phys Lett* (2017) 110(14):143511. doi:10.1063/1.4979543

11. Liu Y, Li K, Jia Y, Hao Y, Gong S, Guo YJ. Wideband RCS Reduction of a Slot Array Antenna Using Polarization Conversion Metasurfaces. *IEEE Trans Antennas Propagat* (2016) 64(1):326–31. doi:10.1109/TAP.2015.2497352

12. Liu Z, Liu S, Bornemann J, Zhao X, Kong X, Huang Z, et al. A Low-RCS, High-GBP Fabry-Perot Antenna with Embedded Chessboard Polarization Conversion Metasurface. *IEEE Access* (2020) 8:80183–94. doi:10.1109/ACCESS.2020.2990602

13. Pandit S, Mohan A, Ray P. Low-RCS Low-Profile Four-Element MIMO Antenna Using Polarization Conversion Metasurface. *Antennas Wirel Propag Lett* (2020) 19(2):2102–6. doi:10.1109/LAWP.2020.3023454

14. Li K, Liu Y, Jia Y, Guo YJ. A Circularly Polarized High-Gain Antenna with Low RCS over a Wideband Using Chessboard Polarization Conversion Metasurfaces. *IEEE Trans Antennas Propagat* (2017) 65(8):4288–92. doi:10.1109/TAP.2017.2710231

15. Zhang W, Liu Y, Jia Y. Circularly Polarized Antenna Array with Low RCS Using Metasurface-Inspired Antenna Units. *Antennas Wirel Propag Lett* (2019) 18(7):1453–7. doi:10.1109/LAWP.2019.2919716

16. Xie B, Tang K, Cheng H, Liu Z, Chen S, Tian J. Coding Acoustic Metasurfaces. *Adv Mater* (2017) 29(6):1603507. doi:10.1002/adma.201603507

17. Cui TJ, Qi MQ, Wan X, Zhao J, Cheng Q. Coding Metamaterials, Digital Metamaterials and Programmable Metamaterials. *Light Sci Appl* (2014) 3(10):e218. doi:10.1038/lsa.2014.99

DATA AVAILABILITY STATEMENT

The original contributions presented in the study are included in the article/Supplementary Material, further inquiries can be directed to the corresponding authors.

AUTHOR CONTRIBUTIONS

All authors listed have made a substantial, direct, and intellectual contribution to the work and approved it for publication.

FUNDING